PCCP

Accepted Manuscript

ROYAL SOCIETY OF CHEMISTRY

www.rsc.org/pccp

Ab initio electronic structure study of a model water splitting dimer complex

Amendra Fernando and Christine M. Aikens*

Department of Chemistry, Kansas State University, Manhattan, Kansas 66506, United States

*cmaikens@ksu.edu

Abstract

A model manganese dimer electrocatalyst bridged by μ-OH ligands is used to investigate changes in spin states that may occur during water oxidation. We have employed restricted open-shell Hartree-Fock (ROHF), second-order Møller-Plesset perturbation theory (MP2), complete active space self-consistent field (CASSCF), and multireference second-order Møller-Plesset perturbation theory (MRMP2) calculations to investigate this system. Multiconfigurational methods like CASSCF and MRMP2 are appropriate methods to study these systems with antiferromagentically-coupled electrons. Orbital occupations and distributions have been closely analyzed to understand the electronic details and contributions to the water splitting from manganese and oxygen atoms. The presence of Mn(IV)O$^{\bullet}$ radical moieties has been observed in this catalytic pathway. Multiple nearly degenerate excited states were found close to the ground state in all structures. This suggests competing potential energy landscapes near the ground state may influence the reactivity of manganese complexes such as the dimers studied in this work.

Introduction

Water splitting has been a popular topic over the past few decades as a clean and sustainable way to produce hydrogen. In green plants and in cyanobacteria, the oxygen evolving complex (OEC) of photosystem II (PSII) catalyzes the water oxidation reaction. The active site

of the OEC consists of a $CaMn_4O_5$ cuboidal structure and there have been many extensive theoretical and experimental studies related to determining its electronic structure, properties, oxidative activation and mechanism of water oxidation.[1-12]

Inspired by this cuboidal structure, many synthetic and model catalysts have been proposed that contain high-valent multinuclear manganese μ-oxo bridged complexes.[13-23] The first reports of water oxidation by a dimanganese complex date back to 1985 when Ashmawy and coworkers[13] synthesized a $[\{Mn(salpd)(H_2O)\}_2][ClO_4]_2$ [salpd = propane-l,3-diylbis (salicylideneiminate)] complex that evolves oxygen when irradiated in the presence of a p-benzoquinone. Watkinson and coworkers[14] also reported a dinuclear manganese complex that evolves O_2 in the presence of a p-benzoquinone in 1994. The first functional model of a μ-oxo bridged manganese dimer ($[H_2O(terpy)Mn(O)_2Mn(terpy)OH_2](NO_3)_3$) was reported by Limburg *et al*.[15] This compound is capable of catalyzing the oxygen evolution reaction similarly to the OEC. Collomb and coworkers[16] synthesized this compound independently at the same time as Limburg and coworkers. Formation of a Mn(V)=O species during O-O bridging was first reported by Naruta *et al*.[17] with a porphyrin type Mn(III) dimer. A four electron water oxidation reaction catalyst ($[Mn_2(mcbpen)_2(H_2O)_2](ClO_4)_2$) (mcbpen = *N*-methyl-*N'*-carboxymethyl-*N,N'*-bis(2-pyridylmethyl)ethane-1,2-diamine) synthesized by Poulsen *et al*.[18] has been reported to generate oxygen with the presence of a tert-butylhydrogenperoxide as an oxidant. These μ-oxo bridged manganese complexes for water oxidation have been reviewed thoroughly by Mullins,[19] Liu,[20] Yagi,[21] Mukhopadhyay,[22] and Wu *et al*.[23]

Electronic structure, charge distribution, and spin coupling of manganese μ-oxo compounds surrounded by triazacyclonoane and acetate have been studied in detail by Zhao and coworkers.[24] Their calculated charge distribution showed strong metal-ligand covalency.

Blomberg *et al*.[25] reported a theoretical study of a number of model manganese compounds including μ-oxo bridged manganese complexes. With hybrid density functional theory (DFT) calculations even without using formally correct spin coupling, they were able to reproduce the experimentally known preference for antiferromagnetic coupling between manganese spins. One interesting finding is that because of the small difference in electronic structure between high spin and low spin states, the optimized geometries for these two states were identical.[25] McGrady and coworkers[26] studied the structural and electronic properties of reduction and oxidation of a peroxo-bridged Mn dimer ($Mn_2(\mu\text{-}O)_2(\mu\text{-}O_2)(NH_3)_6^{2+}$). They reported that reductive cleavage of the O-O σ bond is favorable when the manganese centers are antiferromagentically coupled and that ferromagnetic coupling of the manganese centers favors the oxidative formation of the π component of the O-O bond.[26] Lundberg *et al*.[27] have also investigated the μ-oxo bridged manganese dimer ($[H_2O(terpy)Mn(O)_2Mn(terpy)OH_2](NO_3)_3$) to find out the requirements for O-O bond formation in manganese complexes. They determined that the active synthetic catalyst forms a stable Mn(IV) oxyl radical state rather than the Mn(V)-oxo state.[27] A very recent paper by Zhou *et al*.[28] indicates that the aqua ligand environment has an almost symmetric influence on the Mn(III) and Mn(IV) centers even with the hydrogen bonds considered explicitly.

It is known that some 3d transition metals such as Mn show a poor overlap between the 3d and ligand orbitals.[29] This results in orbital near degeneracies and nondynamical correlations.[29] So, the applicability of DFT methods to account for these electron correlations remains questionable. The systems with 3d orbitals also give rise to several low-lying excited states of various multiplicities, which results in surface crossing effects. Such systems with near degenerate electronic states may have antiferromagnetic coupling of Mn atoms.[29] Busch *et al*.[30] have studied a system based on high spin states in a ferromagnetic arrangement that can be

treated by standard DFT methods. However, the potential antiferromagnetic coupling in these systems can be most appropriately described by multi-determinantal wave function representations. Multi-configurational wave function-based methods like complete active space self-consistent field (CASSCF) and multireference 2nd order Møller-Plesset perturbation theory (MRMP2) are methods that can be used in this type of calculation. Choosing the active space for this type of calculation is very important. Electrons and orbitals involved should include those necessary to treat all the important bonding features yet should not be unnecessarily large because they need to remain computationally tractable.

Very few studies have been reported using CASSCF calculations on ligated manganese compounds. Among them, Mn(salen) complex is a popular system that has a high-yield catalytic activity towards enantioselective epoxidation of unfunctionalized olefins. A debatable question with these Mn(salen) complexes is the relative stability of the singlet, triplet and quintet states. Sears *et al*.[29] and Ivanic *et al*.[31] reported a CASSCF study of a model oxoMn(salen) complex to address this issue. Ivanic *et al*.[31] first studied the system with 12 electrons in 11 active space orbitals (CASSCF(12/11)); later, Sears and coworkers[29] used CASSCF(8/7) to study this system. This smaller active space was chosen after examining the unrestricted Hartree-Fock (UHF) natural orbital occupation numbers. Their reports indicated a closed shell singlet as the ground state and that the triplet states are around 3 kcal mol^{-1} higher in energy whereas a quintet state lies at a little more than 40 kcal mol^{-1}. The relative energies calculated using different active spaces differed by 0.5 kcal mol^{-1} for all the states except for the quintet state whose difference was 1.4 kcal mol^{-1}. It is noteworthy that their UHF solutions to the calculations were highly spin-contaminated. In 2014, Wouters and coworkers[32] studied this system with the density matrix renormalization group (DMRG) method with 28 electrons in 22 orbitals. Inclusion of such a

large active space is feasible with the DMRG numerical technique. In comparison with previous results, they found that the triplet is 5 kcal mol^{-1} more stable than the singlet state whereas the quintet lies 12-14 kcal mol^{-1} higher than the singlet state.

With recent advances in the DMRG method, Kurashige and coworkers[33] computed the many-electron wavefunctions of the OEC of PSII with more than 10^{18} quantum degrees of freedom. They confirmed that the S_1 state of the OEC is in the Mn^{III} Mn^{IV} Mn^{IV} Mn^{III} oxidation state that has been established previously; furthermore, they identified multiple low-lying energy states near the S_1 state. The active space they chose for the DMRG-CASSCF calculations is 44 electrons in 35 orbitals.

Other work has also been performed on manganese and manganese-calcium cubane systems related to the OEC of PSII. Numerous recent studies have examined the electronic structure of these systems using high-spin and broken-symmetry DFT calculations. For example, Yamaguchi and coworkers[34] employed UB3LYP and UBHandHLYP calculations to investigate the mixed valance $Ca_4Mn_4O_4X(H_2O)_4$ (X=OH or O) complex. The authors indicated that the degree of symmetry breaking of the Mn-O-Mn bond is not significant with these levels of theory whereas it is predicted to be higher with other hybrid DFT methods. Yamaguchi *et al*.[35] also reported a study of the mixed valance configurations of Mn_5O_5, $CaMn_4O_5$, and $Ca_2Mn_3O_5$ complexes with UB3LYP calculations. The computational results with Mn_5O_5 demonstrated the instability of the uniform-valance structure of $Mn(III)_5O_5$ due to the Jahn-Teller effect of trivalent Mn ion affording a mixed-valance configuration. Krewald *et al*.[36] investigated a high-valent $Mn(IV)_3CaO_4$ complex and demonstrated that the these systems have a ground state with spin 9/2. Recently, Krewald[37] and coworkers have shown that only a high-valent scheme with

$Mn(III)_3Mn(IV)$ for the S_0 state up to $Mn(IV)_4$ for the S_3 state can account for the observed spectroscopic data of the semi-stable intermediate states.

These studies with DFT (high spin and broken symmetry approaches) as well as multireference and multiconfiguration methods show the complexity of orbital configuration in manganese and how the surrounding ligand environment plays a major role in describing the chemistry of these systems. These complexes are capable of releasing oxygen electrochemically, photochemically, and in the presence of primary oxidants. In the present study we examine a model catalyst proposed by Busch *et al*.[30] The model catalyst consists of two manganese atoms with a simplified version of the acetylacetonate ligand (in which methyl is replaced by hydrogen) on each atom (structure **1** in Figure 1). The purpose of the selection of this model compound is valuable as the two manganese atoms are surrounded by six oxygen atoms, which is similar in that regard to a bulk MnO_2 surface. Capping the manganese atoms with the acetylacetonate ligand ensures that the catalyst is governed towards a direct coupling of two radical moieties. Furthermore, the starting structure with two aqua ligands on top of manganese atoms represents a bulk manganese oxide immersed in a neutral medium with aqua ligands adsorbed to the surface. These factors lead us to conclude that the selected model system is capable of mimicking the actual bulk oxide surface to a satisfactory degree. A synthetic organometallic compound with a similar skeleton to this model catalyst has also been reported as an enhanced magnetic cooler by Manoli and coworkers.[38] The resting state of the catalyst exhibits two water molecules ligated to Mn(III) atoms and these Mn atoms are bridged by hydroxyl groups to balance the neutral charge of the catalyst. The catalytic mechanism proposed[30] is a general direct coupling pathway through Mn-O$^{\bullet}$ radical species that consists of electrochemical steps and chemical steps. It should be noted this radical species is predicted in our current work to be a Mn(IV)-O$^{\bullet}$ group. This will be

discussed in detail in the results and discussion. Each electrochemical step experiences a proton coupled electron transfer (PCET) reaction similar to the OEC of PSII. This type of direct coupling reactions via adjacent oxo radicals has been proposed in ruthenium blue dimer[39, 40] and cobalt oxide catalyst[41] water oxidation systems. A reference system of TyrOH/TyrO$^{\bullet}$ has been used, which has a reduction potential of 0.94 V relative to the normal hydrogen electrode (NHE). The theoretical water oxidation potential value is around 1.23 V with respect to the NHE. This simplified theoretical catalyst system mimics the water oxidation process in a Mn dimer compound.

In this study, we employ both multiconfigurational and mutireference methods to investigate the electronic structure and energetics of this system. These higher levels of theory can account for a detailed description of underlying electronic states that contribute to the catalyst cycle. The primary focus of this study is to observe the orbital configurations that contribute at different stages of this direct-coupling pathway and provide detailed understanding of the electronic states at each stage of the catalytic cycle. We also acknowledge to the readers that these ab initio methods also have their own limitations: in order to accurately address the system of interest we have to carefully select the active space in multiconfigurational calculations. Even with current computational power it is not feasible to include all the valance electrons in this system. Nonetheless, we believe our investigation of electronic excited states and orbitals involved in such reaction pathway may helpful to increase the knowledge base of catalytic water oxidation systems. We find that many nearly degenerate excited states with different spin are present in these systems.

Computational Methods

All the restricted open-shell Hartree-Fock (ROHF),[42] second-order Møller-Plesset perturbation theory (MP2) using the z-averaged perturbation theory (ZAPT2) approach,[43-45] CASSCF,[46-49] and MRMP2[50-55] calculations in this work employed the code implemented in the General Atomic and Molecular Electronic Structure System (GAMESS) program.[56, 57] We have selected an active space with 8 electrons distributed among 10 orbitals CASSCF(8/10), which is physically motivated for the first cluster shown in our study. These 10 orbitals for the first structure include the five 3d orbitals from both Mn atoms and can account for the important bonding features happening around the two Mn atoms in the structures. We have examined expanding the active space to 12, 14, and 16 active orbitals by adding the doubly occupied ring π orbitals and corresponding ring π^* orbitals to the active space as described below, but the natural orbital occupation numbers obtained were at least 1.95 for the doubly occupied orbitals. Furthermore, orbitals of the bridging hydroxo groups were also included in the active space to check their contribution to the behavior of this system. We included 16 active orbitals and found that the orbitals have occupations of at least 1.98, so they are well represented when included in the doubly occupied space. The CASSCF(8/10) active space is used throughout the calculations unless otherwise mentioned.

Since accuracy and the convergence of CASSCF calculations depend on the initial input orbitals, choosing a good set of orbitals is always important. In order to improve SCF orbitals as good starting molecular orbitals, several methods available in GAMESS have been used. For example, generating valance virtual orbitals (VVOs), getting a more localized set of occupied orbitals while retaining symmetry using a Boys localization procedure[58] using a symmetry localization approach implemented in GAMESS, or a combination of these methods have been

used. The initial set of orbitals was carefully analyzed and reordered as necessary to find the optimal set of orbitals for each structure. All the calculations executed in this study use a triple zeta valance basis set with d and p polarization functions (TZVP).[59, 60] Single point MRMP2 calculations have been performed in order to get better estimates of the relative energies where necessary. Orbital diagrams reported in all the figures have been calculated with a contour value of 0.03.

Results and discussion

All the intermediate states in the reaction pathway are initially optimized with ROHF for high-spin states using a TZVP basis set (Figure 1). This catalytic cycle was previously reported in Ref. 30 using the B3LYP/6-311++G level of theory. The cycle consists of four electrochemical steps, in which a proton and electron are removed from the Mn complex, and three chemical steps. The two aqua ligands attached to the top of the structure **1** undergo four consecutive dehydrogenations in four electrochemical steps to form structure **5** with two Mn(IV)-O$^{\bullet}$ radical groups. The two radical oxo groups attack each other and generate the O-O bridge on structure **6**. With two consecutive water addition reactions we can break the two Mn-O bonds and extract O_2 from the catalyst. Structures **1-5** have 86 doubly occupied orbitals and structures **6** and **7** possess 85 and 90 doubly occupied orbitals, respectively.

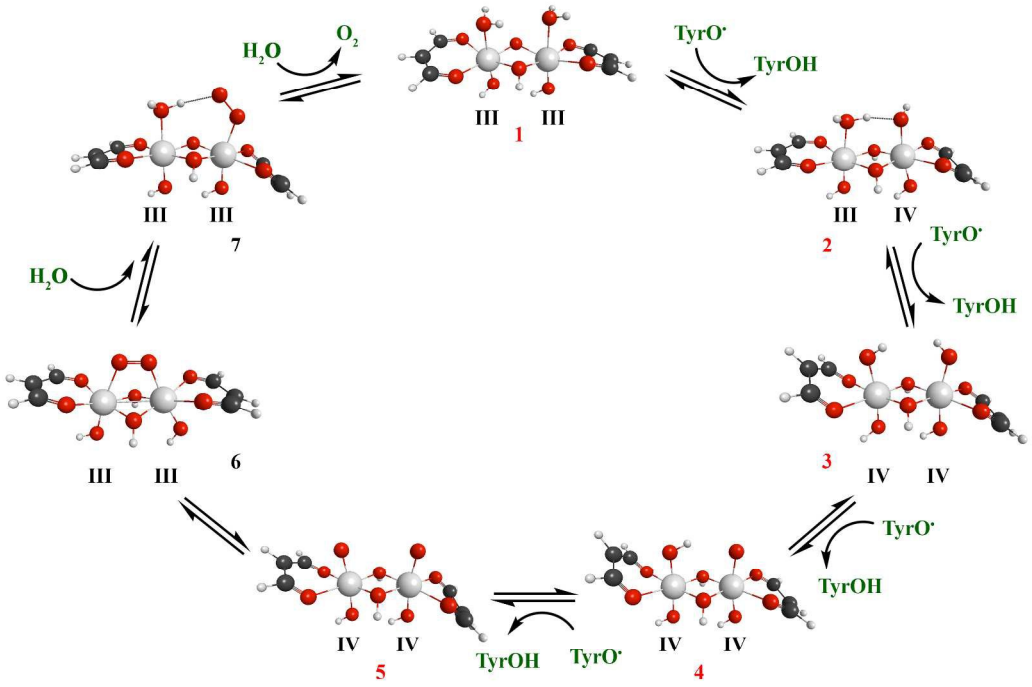

Figure 1. ROHF/TZVP optimized structures for the mechanism reported in Ref. 30. Red numbers indicate the electrochemical pathway and the black numbered structures are generated from purely chemical steps. Small white spheres represent hydrogen atoms and large grey spheres represent manganese atoms. Carbon and oxygen atoms are represented by black and red spheres. This color code is used in all figures.

We have employed MP2 level single point energy calculations on the high spin states of ROHF optimized structures of the catalyst. A comparison of these reaction energies is given in Figure 2. The reaction energy pattern for the catalytic cycle shows similar behavior with both levels of theory. After the formation of Mn(IV)-O$^{\bullet}$ bonds (structure **5**), the chemical step of forming the O-O bond (structure **6**) is a downhill reaction. The most positive reaction energy difference of the cycle is found between structures **6** and **7**, where attack of a water molecule on

the peroxo bridged structure occurs. The reaction energies between structures **4**, **5**, and **6** hints at the flexibility of the direct coupling of the oxo radicals. Except for the catalyst regeneration step (**7** to **1**), ROHF calculations generally overestimate the relative energies of the structures compared to the MP2 single point energies.

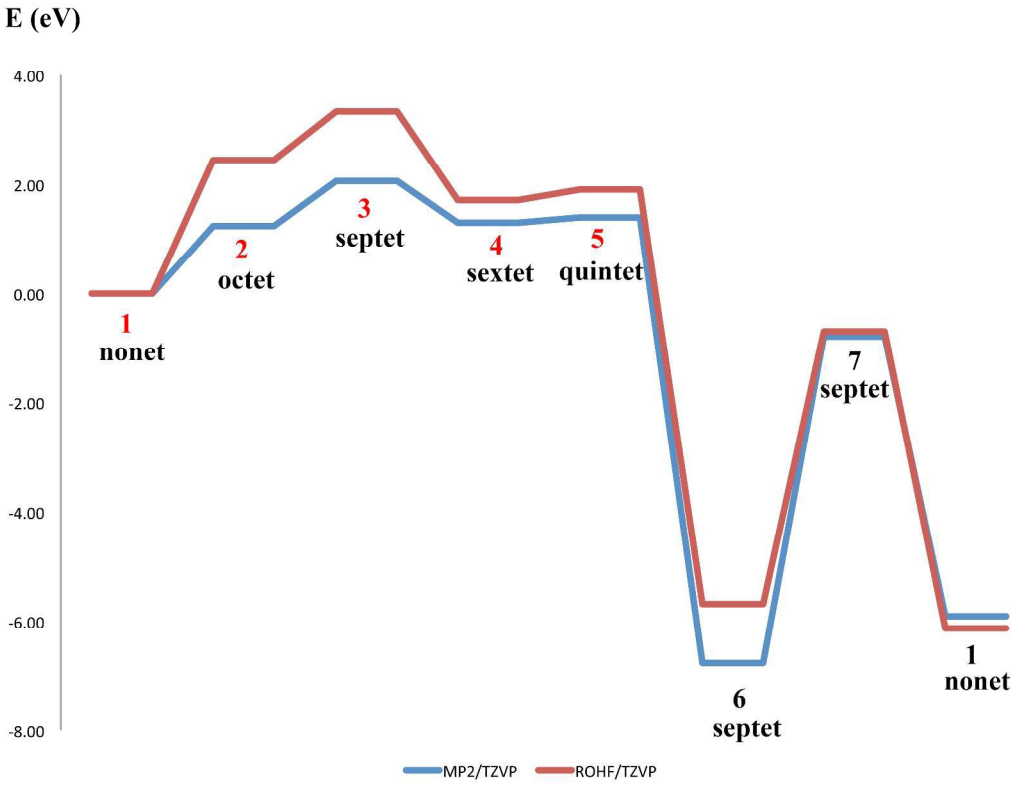

Figure 2. Reaction energies (eV) of the high spin states of the catalyst cycle

All of these structures have C_1 symmetry and possess a pseudo-octahedral geometry around the Mn atoms. The ligands around the manganese atoms show either bent or twisted conformations in structures **1** - **7** and they are not in plane with the μ-hydroxo bonds. With previous B3LYP/6-311++G and BLYP/6-311++G results, the highest thermodynamic energy gap was observed between structures **3** and **4**.[30] In that work, the reaction goes uphill until the formation of structure **5** and then goes downhill to regenerate the catalyst whereas in the current

work with ROHF and MP2, the reaction goes uphill to form structure **3** and then proceeds downhill to structure **4**. The next sections provide detailed descriptions of the electronic states and orbitals for each structure together with a comparison of the ROHF, CASSCF, and previous DFT calculations.

*Structure **1***

In structure **1**, the eight unpaired electrons in the nonet state occupy eight d-based orbitals of the two Mn atoms with two Mn d-based LUMOs. The singly occupied molecular orbitals (SOMOs) are very important as they depict the chemistry occurring around Mn. Orbitals 87 - 94 represent these singly occupied d orbitals optimized with ROHF (Figure 3). We also investigated the unrestricted Hartree-Fock (UHF)[61] orbitals for structure **1** (Figures S1 to S4 in Supporting Information). In the UHF calculations, singly occupied alpha electrons with a high percentage of manganese d orbitals were seen in the lower energy occupied space (orbitals 50-62). Corresponding beta orbitals were not present, so the overall spin density was found to be four electrons on each Mn atom using both Mulliken and Löwdin partitioning schemes. Overall, differences in orbital occupation were noted for the structures examined in this work. The S^2 value for structure **1** was found to be 20.121 (compared to the idealized value of 20), indicating some spin contamination. Spin contamination was also found to be an issue in previous UHF calculations on Mn complexes,[29] so the unrestricted calculations will not be further discussed in this work.

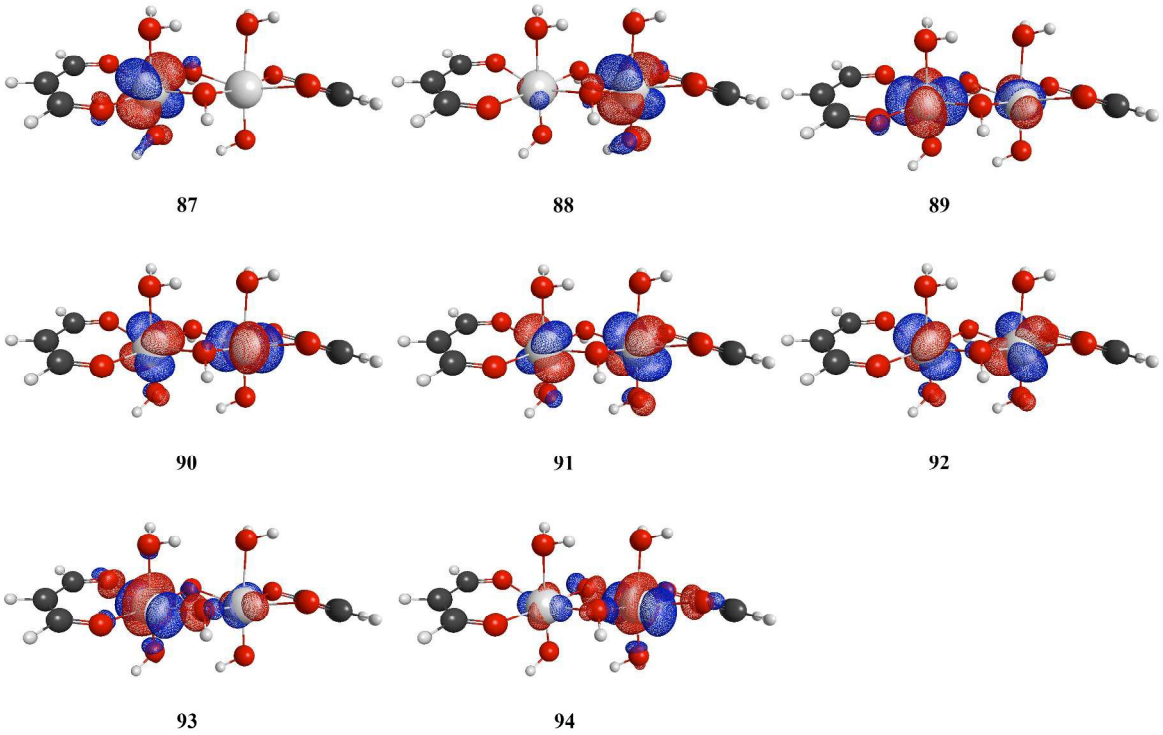

Figure 3. ROHF/TZVP SOMOs of structure **1**

Core orbitals 85 and 86 (Figure 4) also have a significant role in the electronic structure. In structure **1** they are doubly occupied orbitals; in structure **2** and onwards we see that these orbitals change their occupancy. These orbitals represent a ring π orbital delocalized over three carbon atoms with contributions from the p orbitals of the two oxygen atoms in the ligand. These orbitals are hereafter labeled as $R\pi_1$ and $R\pi_2$ (ring π orbitals). This type of ring π orbital exhibits a key role in oxo-Mn(salen) complexes[29, 31] where electron transfer occurs in ring π orbitals to non-bonding axial Mn-O π orbitals in excited states.

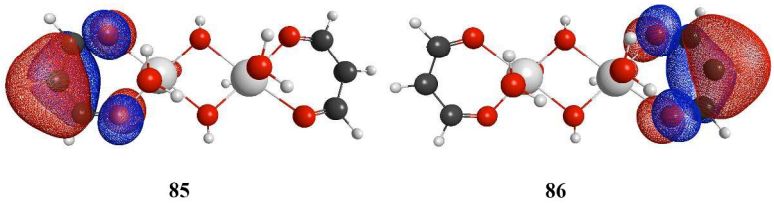

Figure 4. ROHF/TZVP doubly occupied $R\pi_1$ and $R\pi_2$ orbitals of structure **1**

Initial orbitals for CASSCF(8,10) calculations were taken from the ROHF orbitals. In this case convergence was obtained without difficulty. A different spatial distribution of orbitals with the CASSCF wave function is observed. These eight singly occupied Mn d natural orbitals are shown in Figure 5. The two unoccupied natural orbitals in the active space, 95 and 96, also show d orbital character (Figure 5). Doubly occupied orbitals 85 and 86 have $R\pi_1$ and $R\pi_2$ character similar to the ROHF orbitals shown in Figure 4. The natural orbital occupation numbers (NOONs) are essentially 1 or 0 for singly occupied or unoccupied orbitals, respectively.

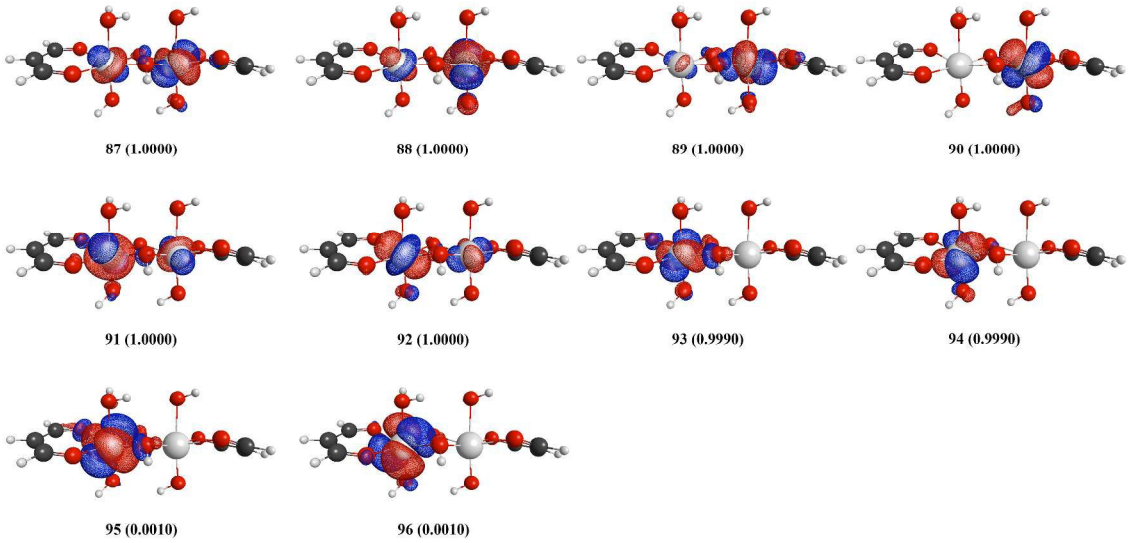

Figure 5. CASSCF(8,10)/TZVP active space natural orbitals of structure **1** (natural orbital occupation numbers (NOONs) are given in parentheses)

The structure did not change drastically in going from the ROHF to the CASSCF level of theory. All eight Mn-O bonds around the two Mn centers changed within a 0.001 Å range. Structure **1** was optimized with different multiplicities. The same initial SCF orbitals were used for other multiplicities as the nonet orbitals are similar between ROHF and CASSCF. There were no structural differences observed in these multiplicities within 0.001 Å. Relative energies of these multiplicities are given in Table 1.

Table 1. Relative CASSCF energies of electronic states for structure **1**

Multiplicities	CASSCF	
	kcal mol^{-1}	cm^{-1}
Triplet	0.035	12.2
Quintet	0.028	9.8
Septet	0.020	7.0
Nonet	0.000	0.0

CASSCF calculations indicate the existence of many low-lying excited states. A CASSCF calculation at the optimized nonet geometry yields the high spin nonet state as the lowest energy state. The previous DFT results also predict the high spin nonet as the lowest energy state.[30] A CASSCF septet calculation at the optimized septet geometry yields an energy of 0.020 kcal mol^{-1} above the nonet state. A CASSCF calculation at the optimized quintet state gives a relative energy of 0.028 kcal mol^{-1}, and a similar CASSCF calculation for the triplet state yields 0.035 kcal mol^{-1}. Even though the high spin electronic state with 8 unpaired electrons is predicted to be the ground state, all of these other states are essentially degenerate. It should also be noted that the orbitals for these 8 unpaired electrons arise mostly from contributions of d orbitals on the two manganese atoms; very small contributions of orbitals from the bridging hydroxo groups are observed in the unpaired electrons of structure **1** and the other structures discussed below. To account for contributions from the hydroxo bridges, we included these

orbitals in the active space; however, all natural orbital occupation numbers were found to be at least 1.98, and thus for the remainder of this work they will be treated in the doubly occupied space.

This degeneracy of the electronic states can be observed in other structures of the reaction mechanism, producing competitive potential energy landscapes. Existence of these multiple nearly-degenerate potential energy landscapes near the ground state for the OEC of PSII have been shown recently with DMRG calculations, thus giving a very reactive environment for the manganese water oxidation systems.[33] For all of the lower spin multiplicities, the NOONs are essentially 1 or 0, indicating that the electrons remain unpaired.

*Structure **2***

Dehydrogenation leads to a Mn(IV) oxidation state in one of the manganese atoms in structure **2**. CASSCF optimization of structure **2** with different multiplicities reveals a low-lying sextet as the ground state. The octet is calculated to be 0.333 kcal mol^{-1} higher in energy than the sextet state. The natural orbitals used in the active space of the sextet state of structure **2** are provided in Figure 6 and those used in the octet state are given in the Supporting Information (SI), Figure S5. The doublet and quartet states are 0.414 and 0.056 kcal mol^{-1} higher in energy than the sextet state, respectively (Table 2). There are no apparent differences in the structures of these states. As seen for structure **1**, the four spin states are essentially degenerate. To check the effect of the active space on the state ordering, we also performed CASSCF calculations without the three essentially unoccupied orbitals 94-96, leading to a (7,7) active space. Again, the sextet state was found to be the lowest in energy. Even though CASSCF calculations are capable of accurately addressing electronic exchange and nondynamical correlations, they do a poor job of accounting for dynamical electron correlations. To see if the system is drastically affected by

these dynamical correlations, we employed MRMP2(7,10) calculations on structure **2**. In comparison, previous DFT calculations have predicted the octet state as the lowest energy state.[30]

Table 2. Relative CASSCF and MRMP2 energies of different states for structure **2**

Multiplicities	CASSCF		MRMP2	
	kcal mol^{-1}	cm^{-1}	kcal mol^{-1}	cm^{-1}
Doublet	0.414	144.8	0.017	6.0
Quartet	0.056	19.6	0.002	0.7
Sextet	0.000	0.0	0.000	0.0
Octet	0.333	116.5	0.014	4.9

MRMP2 single point energies (Table 2) for the doublet, quartet, sextet, and octet were obtained at the CASSCF optimized geometries for their respective multiplicities. Initial orbitals were taken from the CASSCF wavefunction of structure **2** for each respective multiplicity. We have found that there are no large differences in energy with the MRMP2 level of theory, although the relative energies of the doublet, quartet, and octet states decrease somewhat. MRMP2 reproduced the sextet state as the ground state for structure **2** and the energy ordering of the remaining states is the same as from the CASSCF prediction. It is interesting to note that the CASSCF and MRMP2 calculations do not agree with predictions from a phenomenological Heisenberg-Dirac-Van Vleck (HDVV) Hamiltonian, which would predict either the ferromagnetic (octet) or antiferromagnetic (doublet) states to be lowest in energy depending on the value of the exchange constant J with a spacing of E(S-1)-E(S)=2JS (where S is the total spin quantum number of the system). It should also be noted that previous B3LYP and BLYP calculations also do not predict state intervals according to HDVV predictions; for structure **1**, the singlet and quintet states were predicted to lie above the nonet state with the triplet highest in

energy, and for structure **2**, although the octet was predicted to lie lowest in energy, the other states were not arranged according to HDVV predictions.[30]

Interesting orbital configurations were observed when hydrogen was abstracted from water ligated on Mn to form an O-H bond in structure **2**. A singly occupied d orbital has now lowered its energy to the doubly occupied core orbital space. (This d orbital 69 is given in the SI (Figure S6) and it has been compared with a range of orbitals in structure **1** to check the existence of this d orbital. We did not observe a similar kind of d orbital in structure **1** and attribute this to a lowering of a singly occupied d orbital into the doubly occupied core orbital space.) In addition, a higher energy ring π ($R\pi_2$) orbital on the side of the molecule that has undergone hydrogen abstraction is now singly occupied. We have also examined active spaces in which both ring π orbitals are active orbitals; however, one always remains doubly occupied (NOON > 1.97) and one stays singly occupied (NOON ~ 1.00). We hypothesize that removal of electron population in this ring π orbital is the cause for out-of-plane bending of the respective ligand that has been observed in this structure. The doubly occupied ring π orbital 86 and the singly occupied ring π orbital along with the remainder of the orbitals are given in Figure 6. Singly occupied orbitals 87 and 92 show a very small p orbital contribution from the dehydrogenated aqua ligand. We also observed that there is very little contribution from bridged OH groups. CASSCF calculations were able to find the remaining unoccupied d orbitals in the active space. In comparison to the active space orbital configurations observed with the structure **1**, structure **2** possesses a different set of orbitals based on the Mn d orbitals. In this structure, the change in number of unpaired electrons does not solely affect the two manganese atoms; the contribution of the ring π orbital to the active space indicates that ligand framework and its ability to transfer an electron to aid the hydrogen removal process is also an important factor.

Since the character of the orbitals in the active space differs for structures **1** and **2**, the CASSCF energies of these systems cannot be directly compared.

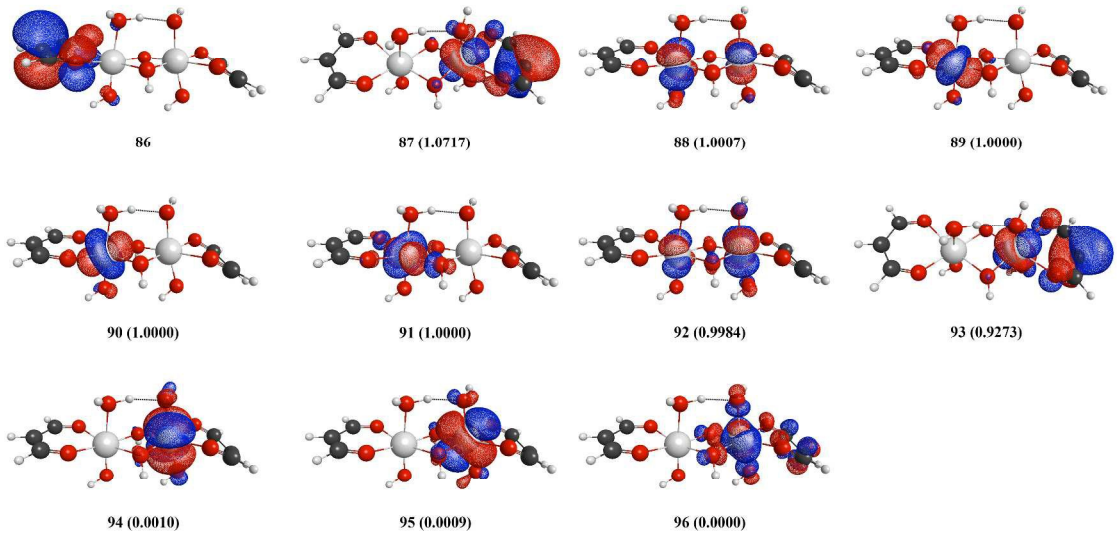

Figure 6. CASSCF(7,10)/TZVP natural orbitals 86-96 in the sextet state of structure **2**. Orbital 86 is a doubly occupied core orbital, and the other ten orbitals are included in the active space.

*Structure **3***

This species has had two hydrogens abstracted from the resting state of the catalyst and two manganese atoms are now in the Mn(IV) oxidation state. As mentioned earlier, when the multiplicities were changed in structures **1** and **2**, there were no geometric differences within 0.001 Å. The CASSCF geometry optimization of the septet state and a single point CASSCF energy calculation at the ROHF geometry for the septet state of structure **3** gave essentially the same energy. Similarly, the geometries for the structures with different multiplicities are not expected to vary greatly. Thus, we used CASSCF single point energies for all the multiplicities of structure **3** at the optimized CASSCF septet geometry to compare in Table 4. The previous DFT results predicted the stability order with the BLYP functional as $E_{septet}<E_{singlet}<E_{quintet}<E_{triplet}$

and with the B3LYP functional as $E_{septet}<E_{quintet}<E_{singlet}=E_{triplet}$, where the septet state is predicted to be the most stable state with both of these functionals.[30] In contrast, the CASSCF calculations suggest the low spin triplet state as the most stable ground state with the septet being 0.28 kcal mol^{-1} higher in energy. These energy values also suggest near degeneracy among these electronic states.

Table 4. Relative CASSCF energies of different states of structure **3**

Multiplicities	CASSCF	
	kcal mol^{-1}	cm^{-1}
Singlet	0.012	4.2
Triplet	0.000	0.0
Quintet	0.071	24.8
Septet	0.276	96.5

CASSCF natural orbitals reproduced the orbital configuration from ROHF except for reordering and mixing of the orbitals. Orbitals 87 and 88 both now represent $R\pi_1$ and $R\pi_2$ singly occupied orbitals (NOONs of 1.0000) on each side of the ligands (Figure 7). This suggests, consistent with our previous observation, another singly occupied orbital has lowered its energy into the core orbitals leading the doubly occupied $R\pi$ orbital to become a higher energy singly occupied orbital. We extensively investigated this system to find the core d electron in the system but we were unable to positively identify it. The single electron occupations in both of these ring π orbitals in structure **3** cause them to bend out of plane as we hypothesized before for structure **2**.

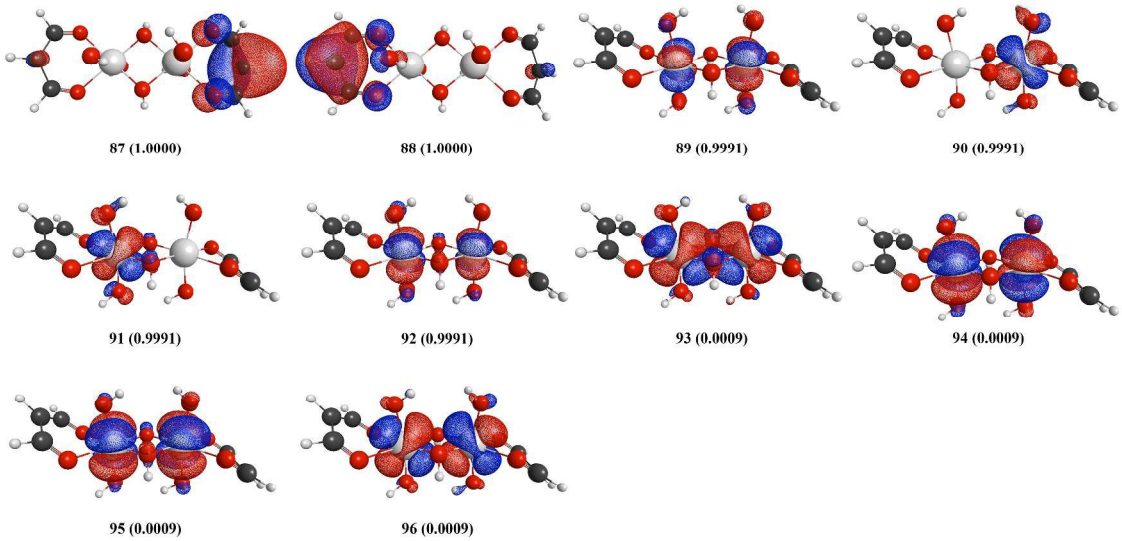

Figure 7. CASSCF(6,10)/TZVP active space natural orbitals of structure **3**

In the singly occupied space starting from orbital 88 to orbital 92 we now see some p orbitals of the two dehydrogenated aqua ligands in the active space contributing to the electronic structure of structure **3**.

*Structure **4***

An important structure in the catalytic cycle is formed when the third hydrogen is abstracted from the initial structure to form an oxo group directly attached to a Mn atom. Formation of an oxo species plays a crucial role in this direct coupling catalytic pathway as the two oxygen atoms combine to form the bridged peroxo group. The BLYP and B3LYP functionals predicted the sextet/quartet and sextet/octet (both spin states are degenerate: sextet and quartet in BLYP and sextet and octet in B3LYP) as the lowest energy states respectively.[30] CASSCF single point energy calculations on structure **4** revealed that the sextet state is not the ground state. The low spin doublet state is the ground state for structure **4** and the sextet state is 5.805 kcal mol^{-1} higher in energy than the doublet state (Table 5). With the formation of this

radical Mn(IV)-O$^{\bullet}$ group, low spin states tend to be lower in energy compared to the high spin electronic states.

Table 5. Relative CASSCF energies of different states of structure **4**

Multiplicities	CASSCF	
	kcal mol^{-1}	cm^{-1}
Doublet	0.000	0.0
Quartet	0.285	99.7
Sextet	5.805	2030.3

Our study shows that the oxygen in the Mn-O bond has radical character, in line with a prediction of Mn(IV)-O$^{\bullet}$ character rather than Mn(V)=O. This is evident from the oxo p orbital contribution in orbital 89 (Figure 8). The singly occupied orbitals 87, 89, 90, and 91 all show contributions from the p orbital of the oxo group. Orbitals 90 and 91 show d orbitals of manganese and π* orbitals between manganese and oxygen. Orbitals 92-96 show LUMOs of structure **4** consisting of manganese d orbitals and π* orbitals between manganese and oxygen atoms.

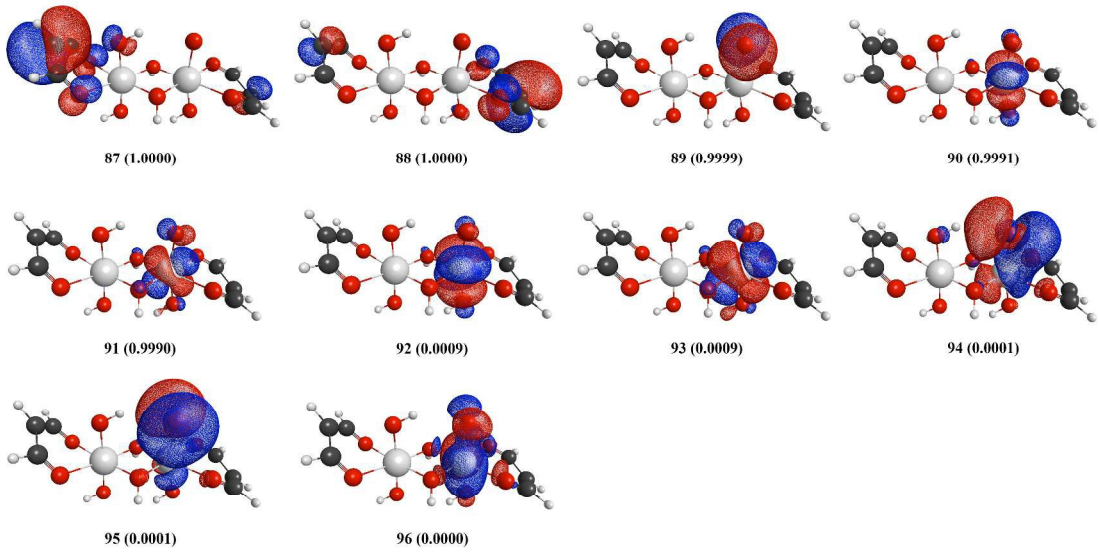

Figure 8. CASSCF(5,10)/TZVP active space natural orbitals of structure **4**

*Structure **5***

Structure **5** possesses two Mn(IV)-O$^{\bullet}$ species. Orbitals 87 and 89 are singly occupied ring π orbitals similar to those in structures **3** and **4** but with more oxygen p orbitals mixing (Figure 9). We were not able to converge structure **5** with an active space of 10 orbitals due to low occupation numbers in the last 4 orbitals. Thus, we selected a smaller active space of 4 electrons in 6 orbitals. We observed a mixing of oxygen p orbitals and ring π orbitals. Generation of another p orbital on the other oxo group can be seen in the active space. Orbitals 88 and 90 both are now singly occupied oxo p orbitals with a slight contribution from ring π orbitals. From structure **5** onwards, singly occupied oxygen p orbitals are also involved in the active space.

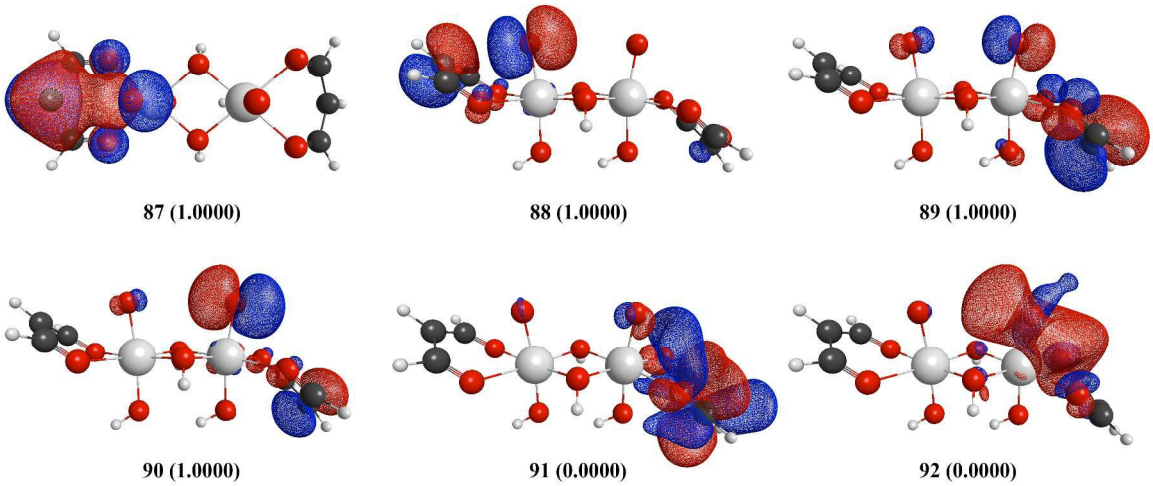

Figure 9. CASSCF(4,6)/TZVP active space natural orbitals of structure **5**

Similar to structure **4**, low spin states tend to be lower in energy with the formation of these higher oxidation states on manganese atoms. Here in structure **5**, the singlet state is the ground state. Single point energy calculations show that the triplet state is 0.002 kcal mol^{-1} higher in energy than the singlet state so these two states are practically degenerate. The quintet state is 0.466 kcal mol^{-1} higher in energy than the ground state. When the structure is optimized at each respective multiplicity, we found the triplet state to be the ground state and the singlet to be 0.009 kcal mol^{-1} higher in energy. Overall, the singlet state and the triplet state of structure **5** are essentially degenerate. In comparison, the quintet state is predicted as the lowest energy state with the B3LYP functional and BLYP predicts the singlet state as the ground state.[30]

*Structure **6***

Going from structure **5** to **6** is a purely chemical step, and the reaction energetics suggest that electrons in oxo p orbitals tend to react favorably to generate structure **6**. This represents the formation of the μ-peroxo bridge between the manganese atoms. The number of electrons in the

system does not change. However, there are a lot of changes in the electronic structure of the system. The σ bond between the two oxygen atoms is now fully formed, which means that this orbital now lies in the doubly occupied subspace. In structure **6,** we now have 85 doubly occupied orbitals where orbital 85 is a ring π orbital similar to previous doubly occupied ring π orbitals (Figure 10). Orbital 86 is a singly occupied ring π orbital. A singly occupied π* orbital between the two bridging oxygen atoms can be seen in orbital 87. Electron filling in these π* orbitals is required for formation of the oxygen molecule. The corresponding π orbital is located in the doubly occupied space. In consequence, the bond order between the two oxygen atoms can be considered to be approximately 1.5. The O-O bond length in structure **6** is around 1.283 Å, which is closer to an oxygen-oxygen double bond than a single bond. A CASSCF relative energy comparison reveals that the triplet state is the ground state for structure **6** (Table 6). This is the same as for structure **5**, so no change in the spin state is required for this chemical step (unlike ROHF or DFT calculations examining high-spin states, which suggested a quintet-to-septet conversion). Overall, the multireference calculations examined in this work suggest that spin-forbidden processes predicted by high-spin calculations may not be truly spin-forbidden, as low-spin states are essentially degenerate to or lower in energy than the high-spin states.

Table 6. Relative CASSCF energies of different states of structure **6**

Multiplicities	CASSCF	
	kcal mol^{-1}	cm^{-1}
Singlet	0.793	277.4
Triplet	0.000	0.0
Quintet	0.488	170.7
Septet	3.156	1103.8

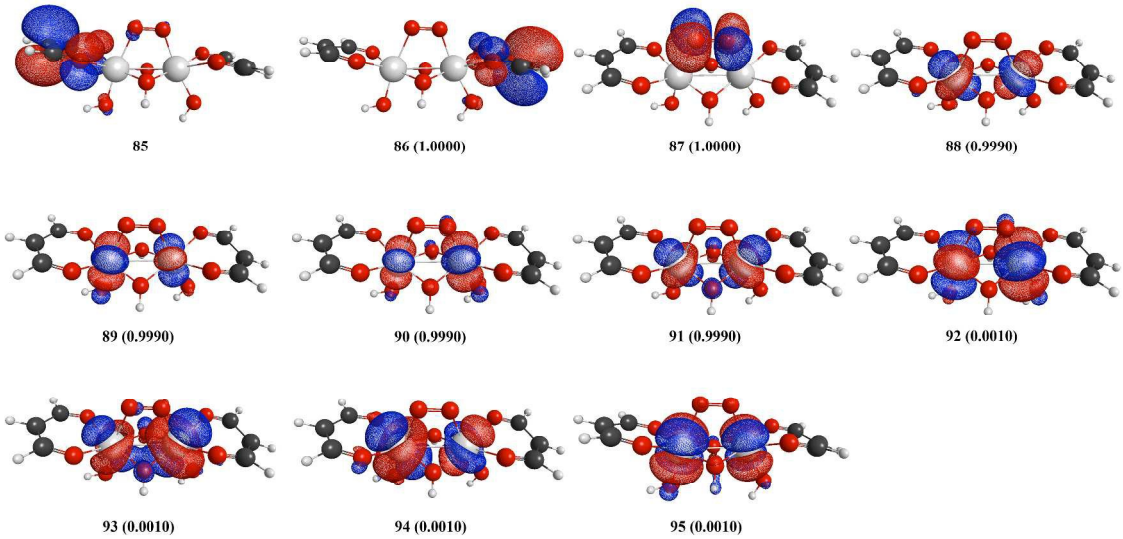

Figure 10. CASSCF(6,10)/TZVP natural orbitals 85-95 of structure **6**

Structure 7

Insertion of a water molecule into structure **6** will break a Mn-O bond but leave O=O still attached to the other manganese atom. The addition of the aqua ligand increases the number of doubly occupied orbitals to 90. Orbital 90 in the septet state of structure **7** is a doubly occupied ring π orbital (Orbital 90 is equal to the ring π orbital 86 in Figure 4). The previously observed singly occupied π* orbital on the bridging O=O can now be seen in orbital 91 (Figure 11). Orbital 92 is a singly occupied ring π orbital. The remaining four electrons are present in singly occupied Mn d orbitals and are shown in Figure 11 with the LUMOs used in the active space. Relative energies for different spin states are given in Table 7, and show that the lowest energy state of **7** is a triplet.

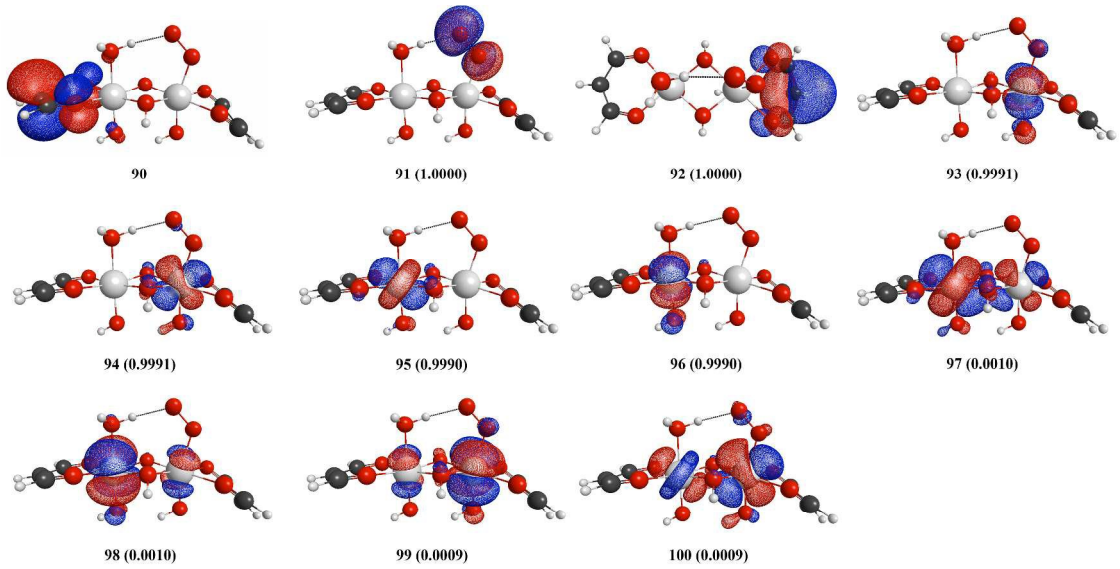

Figure 11. Doubly occupied orbital 90 and CASSCF(6,10)/TZVP natural orbitals 91-100 of structure **7**

Table 7. Relative CASSCF energies of different states in structure **7**

Multiplicities	CASSCF	
	kcal mol^{-1}	cm^{-1}
Singlet	0.395	138.2
Triplet	0.000	0.0
Quintet	0.353	123.5
Septet	2.278	796.7

An incoming water molecule can detach the superoxo group in structure **7** leading back to structure **1**, the resting state of the catalyst. This is a downhill reaction indicating the regeneration of the model catalyst. A transition from **7** in its triplet state to **1** in its nonet state would be spin-forbidden, so it is possible that **7** would actually be present in a higher spin state or that **1** may access a lower spin state. Since the differences in energy between the spin states

are small for each structure examined here, the actual spin state accessed may not be important in this case. In comparison, for both structures **6** and **7**, DFT predicted the septet state as the ground state.[30]

Overall, the low-lying electronic states presented in this model system are an important factor to understand the reactivity of manganese. Nearby ligands also play a key role by changing the singly occupied orbitals present in the system. We also observed that the low spin states tend to be more stable when the electrocatalytic oxygen evolution is in progress in the last stages of the reaction. The contributions from orbitals of the bridging oxo groups to the active space were very small. Formation of Mn(IV)-O$^{\bullet}$ groups in structures **4** and **5** resulted in large contributions from the oxo p orbitals to the active space, thus changing the electronic properties of the structure. It should also be noted that the electron occupation in π^* orbitals is required prior to oxygen removal from the catalyst. As described above, we see that the ligands tend to change orientation with the occupation of the ring π orbitals. With two dehydrogenations yielding structure **3** where two manganese atom are in the Mn(IV) oxidation state, the rings were seen to bend out of the manganese dimer plane. This bend was more pronounced at structure **5** with two Mn(IV)-O$^{\bullet}$ groups. When the oxygen-oxygen bridge is formed, the rings bend in the same direction, making a butterfly-like structure in structure **6**. With the detachment of the oxygen bridge from one manganese atom, this symmetric structure distorts somewhat to yield structure **7**.

Concluding Remarks

In conclusion, we used CASSCF theory to investigate a water splitting reaction mechanism on a model manganese dimer electrocatalyst. Electronic details and contributions to the water splitting from manganese and oxygen atoms involved can be obtained by examining

the occupied orbitals. Apart from the resting state of the catalyst, a singly occupied ring π orbital on the ligands can be seen throughout the catalytic cycle. We also hypothesize that this ring π population may be a reason for the out of plane orientation of the respective ligands. In structure **3** with two Mn(IV) atoms, an out of plane bend of both ligands in opposite directions was observed. This became more pronounced upon formation of Mn(IV) oxidation states on two manganese atoms in structure **5**. However, with the formation of the oxygen-oxygen bridge between the Mn(III) atoms on structure **6**, these ligands tend to bend in the same direction forming a butterfly-like structure, which later distorts with the detachment of the oxo bridge from one manganese atom on structure **7**.

Radical properties of a Mn-O moiety have also been observed in this direct coupling pathway. The p orbital contribution to the active space is observed with the formation of the Mn(IV)-O$^{\bullet}$ group and is much more obvious in structure **5** with two Mn(IV)-O$^{\bullet}$. For structure **5** with two Mn(IV) states, we have observed the prominent contribution of p orbitals of both oxo groups to the singly occupied active space. This then yields the oxo bridge in structure **6**. The π* orbitals were seen to be occupied in the oxygen-oxygen bond in structures **6** and **7**.

With the progress of the catalytic cycle, we also note that low spin states have an improved stability in the later stages of the cycle. However, there are multiple nearly degenerate excited states close to the ground state in all the structures studied here. This is an important factor because spin-forbidden processes predicted from high-spin calculations may not truly be spin-forbidden. In addition, the reaction energies will vary somewhat from those predicted by high-spin calculations. However, since the NOONs of the active orbitals are very close to 2, 1, or 0, and since the energies of the various spin states are typically quite close in energy, this suggests that high-spin calculations may provide a reasonable approximation to reaction

pathways. Nonetheless, this should be verified for other systems. Overall, we believe this detailed electronic investigation may helpful in explaining future studies of manganese-based catalysis.

Supporting Information

Unrestricted Hartree-Fock orbitals for structure **1**. Active space natural orbitals in the octet state of structure **2** and natural core orbital 69 of structure **2**. This information is available free of charge via the Internet at http://pubs.acs.org/.

Acknowledgements

This material is based upon work supported by the National Science Foundation under Grant No. CHE-0955515. C.M.A. also thanks the Alfred P. Sloan Foundation for a Sloan Research Fellowship (2011-2013) and the Camille and Henry Dreyfus Foundation for a Camille Dreyfus Teacher-Scholar Award (2011-2016). The authors thank Dr. Jakub Chalupsky, Prof. Takashi Yanai, Prof. Yuki Kurashige, and Dr. Michael Busch for interesting discussions. The computing for this project was performed on the Beocat Research Cluster at Kansas State University, which is funded in part by NSF grants CNS-1006860, EPS-1006860, and EPS-0919443.

References

1. C. W. Cady, R. H. Crabtree and G. W. Brudvig, *Coord. Chem. Rev.*, 2008, **252**, 444-455.
2. H. Dau, A. Grundmeier, P. Loja and M. Haumann, *Phil. Trans. R. Soc. B*, 2008, **363**, 1237-1244.
3. K. N. Ferreira, T. M. Iverson, K. Maghlaoui, J. Barber and S. Iwata, *Science*, 2004, **303**, 1831-1838.
4. J. P. McEvoy and G. W. Brudvig, *Chem. Rev.*, 2006, **106**, 4455-4483.

5. L. Rapatskiy, N. Cox, A. Savitsky, W. M. Ames, J. Sander, M. M. Nowaczyk, M. Rögner, A. Boussac, F. Neese, J. Messinger and W. Lubitz, *J. Am. Chem. Soc.*, 2012, **134**, 16619-16634.
6. K. Sauer and V. K. Yachandra, *Biochim. Biophys. Acta, Bioenerg.*, 2004, **1655**, 140-148.
7. P. E. M. Siegbahn, *Acc. Chem. Res.*, 2009, **42**, 1871-1880.
8. P. E. M. Siegbahn, *J. Photochem. Photobiol., B*, 2011, **104**, 94-99.
9. P. E. M. Siegbahn, *Phys. Chem. Chem. Phys.*, 2012, **14**, 4849-4856.
10. P. E. M. Siegbahn, *Biochim. Biophys. Acta, Bioenerg.*, 2013, **1827**, 1003-1019.
11. P. E. M. Siegbahn and M. R. A. Blomberg, *J. Chem. Theory Comput.*, 2013, **10**, 268-272.
12. Y. Umena, K. Kawakami, J.-R. Shen and N. Kamiya, *Nature*, 2011, **473**, 55-60.
13. F. M. Ashmawy, C. A. McAuliffe, R. V. Parish and J. Tames, *J. Chem. Soc., Dalton Trans.*, 1985, DOI: 10.1039/DT9850001391, 1391-1397.
14. M. Watkinson, A. Whiting and C. A. McAuliffe, *J. Chem. Soc., Chem. Commun.*, 1994, DOI: 10.1039/C39940002141, 2141-2142.
15. J. Limburg, J. S. Vrettos, L. M. Liable-Sands, A. L. Rheingold, R. H. Crabtree and G. W. Brudvig, *Science*, 1999, **283**, 1524-1527.
16. M.-N. Collomb, A. Deronzier, A. Richardot and J. Pecaut, *New J. Chem.*, 1999, **23**, 351-354.
17. Y. Naruta, M.-a. Sasayama and T. Sasaki, *Angew. Chem. Int. Ed. Engl.*, 1994, **33**, 1839-1841.
18. A. K. Poulsen, A. Rompel and C. J. McKenzie, *Angew. Chem. Int. Ed.*, 2005, **44**, 6916-6920.
19. C. S. Mullins and V. L. Pecoraro, *Coord. Chem. Rev.*, 2008, **252**, 416-443.
20. X. Liu and F. Wang, *Coord. Chem. Rev.*, 2012, **256**, 1115-1136.
21. M. Yagi, A. Syouji, S. Yamada, M. Komi, H. Yamazaki and S. Tajima, *Photochem. Photobiol. Sci.*, 2009, **8**, 139-147.
22. S. Mukhopadhyay, S. K. Mandal, S. Bhaduri and W. H. Armstrong, *Chem. Rev.*, 2004, **104**, 3981-4026.
23. A. J. Wu, J. E. Penner-Hahn and V. L. Pecoraro, *Chem. Rev.*, 2004, **104**, 903-938.
24. X. G. Zhao, W. H. Richardson, J. L. Chen, J. Li, L. Noodleman, H. L. Tsai and D. N. Hendrickson, *Inorg. Chem.*, 1997, **36**, 1198-1217.
25. M. R. A. Blomberg, P. E. M. Siegbahn, S. Styring, G. T. Babcock, B. Åkermark and P. Korall, *J. Am. Chem. Soc.*, 1997, **119**, 8285-8292.
26. J. E. McGrady and R. Stranger, *Inorg. Chem.*, 1999, **38**, 550-558.
27. M. Lundberg, M. R. A. Blomberg and P. E. M. Siegbahn, *Inorg. Chem.*, 2003, **43**, 264-274.
28. T. Zhou, X. Lin and X. Zheng, *J. Chem. Theory Comput.*, 2013, **9**, 1073-1080.
29. J. S. Sears and C. D. Sherrill, *J. Chem. Phys.*, 2006, **124**, 144314.
30. M. Busch, E. Ahlberg and I. Panas, *Phys. Chem. Chem. Phys.*, 2011, **13**, 15069-15076.
31. J. Ivanic, J. R. Collins and S. K. Burt, *J. Phys. Chem. A*, 2004, **108**, 2314-2323.
32. S. Wouters, T. Bogaerts, P. Van Der Voort, V. Van Speybroeck and D. Van Neck, *J. Chem. Phys.*, 2014, **140**, 241103.
33. Y. Kurashige, G. K.-L. Chan and T. Yanai, *Nat Chem*, 2013, **5**, 660-666.
34. K. Yamaguchi, H. Isobe, S. Yamanaka, T. Saito, K. Kanda, M. Shoji, Y. Umena, K. Kawakami, J. R. Shen, N. Kamiya and M. Okumura, *Int. J. Quantum Chem.*, 2013, **113**, 525-541.

35. K. Yamaguchi, Y. Kitagawa, H. Isobe, M. Shoji, S. Yamanaka and M. Okumura, *Polyhedron*, 2013, **57**, 138-149.
36. V. Krewald, F. Neese and D. A. Pantazis, *J. Am. Chem. Soc.*, 2013, **135**, 5726-5739.
37. V. Krewald, M. Retegan, N. Cox, J. Messinger, W. Lubitz, S. DeBeer, F. Neese and D. A. Pantazis, *Chemical Science*, 2015, **6**, 1676-1695.
38. M. Manoli, A. Collins, S. Parsons, A. Candini, M. Evangelisti and E. K. Brechin, *J. Am. Chem. Soc.*, 2008, **130**, 11129-11139.
39. X. Yang and M.-H. Baik, *J. Am. Chem. Soc.*, 2004, **126**, 13222-13223.
40. X. Yang and M.-H. Baik, *J. Am. Chem. Soc.*, 2006, **128**, 7476-7485.
41. L.-P. Wang and T. Van Voorhis, *J. Phys. Chem. Lett.*, 2011, **2**, 2200-2204.
42. C. C. J. Roothaan, *Reviews of Modern Physics*, 1960, **32**, 179-185.
43. C. M. Aikens, G. D. Fletcher, M. W. Schmidt and M. S. Gordon, *J. Chem. Phys.*, 2006, **124**, 014107.
44. T. J. Lee, A. P. Rendell, K. G. Dyall and D. Jayatilaka, *J. Chem. Phys.*, 1994, **100**, 7400-7409.
45. T. J. Lee and D. Jayatilaka, *Chem. Phys. Lett.*, 1993, **201**, 1-10.
46. B. O. Roos, ed. K. P. Lawley, Wiley Interscience, New York, 1987, vol. 69, pp. 339-445.
47. K. Ruedenberg, M. W. Schmidt and M. M. Gilbert, *Chem. Phys.*, 1982, **71**, 51-64.
48. K. Ruedenberg, M. W. Schmidt, M. M. Gilbert and S. T. Elbert, *Chem. Phys.*, 1982, **71**, 65-78.
49. K. Ruedenberg, M. W. Schmidt, M. M. Gilbert and S. T. Elbert, *Chem. Phys.*, 1982, **71**, 41-49.
50. K. Hirao, *Int. J. Quantum Chem.*, 1992, **44**, 517-526.
51. K. Hirao, *Chem. Phys. Lett.*, 1992, **196**, 397-403.
52. K. Hirao, *Chem. Phys. Lett.*, 1992, **190**, 374-380.
53. K. Hirao, *Chem. Phys. Lett.*, 1993, **201**, 59-66.
54. H. Nakano, *Chem. Phys. Lett.*, 1993, **207**, 372-378.
55. H. Nakano, *J. Chem. Phys.*, 1993, **99**, 7983-7992.
56. C. E. Dykstra, G. Frenking, K. S. Kim, G. E. Scuseria, M. S. Gordon and M. W. Schmidt, *Elsevier, Amsterdam*, 2005, 1167-1189.
57. M. W. Schmidt, K. K. Baldridge, J. A. Boatz, S. T. Elbert, M. S. Gordon, J. H. Jensen, S. Koseki, N. Matsunaga, K. A. Nguyen, S. Su, T. L. Windus, M. Dupuis and J. A. Montgomery, *J. Comput. Chem.*, 1993, **14**, 1347-1363.
58. S. F. Boys, ed. P. O. Lowdin, Academic Press, New York, 1966, pp. 253-262.
59. T. H. Dunning, *J. Chem. Phys.*, 1971, **55**, 716-723.
60. A. J. H. Wachters, *J. Chem. Phys.*, 1970, **52**, 1033-1036.
61. J. A. Pople and R. K. Nesbet, *J. Chem. Phys.*, 1954, **22**, 571-572.